



## Research Article

# A new potential green-emitting erbium-activated $\alpha\text{-Na}_3\text{Y}(\text{VO}_4)_2$ nanocrystals for UV-excitable single-phase pc-WLED applications

Linju Ann Jacob<sup>1</sup> · S. Sisira<sup>1</sup> · Kamal P. Mani<sup>1</sup> · Kukku Thomas<sup>1</sup> · Dinu Alexander<sup>1</sup> · P. R. Biju<sup>1</sup> · N. V. Unnikrishnan<sup>1</sup> · Cyriac Joseph<sup>1</sup> 

Received: 22 September 2019 / Accepted: 6 May 2020 / Published online: 14 May 2020  
© Springer Nature Switzerland AG 2020

## Abstract

A potential UV-excitable green-emitting erbium-doped  $\alpha\text{-Na}_3\text{Y}(\text{VO}_4)_2$  nanocrystalline phosphor has been successfully synthesized via facile citrate-based solution combustion method. The structural characterization of the sample was carried out using X-ray diffraction, TEM, HRTEM, SAED, EDS and FTIR analysis. The phosphor exhibits green emission at 523 nm and 552 nm, which correspond to  ${}^2\text{H}_{11/2} \rightarrow {}^4\text{I}_{15/2}$  and  ${}^4\text{S}_{3/2} \rightarrow {}^4\text{I}_{15/2}$  transitions of  $\text{Er}^{3+}$ , respectively. The energy transfer mechanism among  $\text{Er}^{3+}$  ions and the concentration mechanism have been studied. The optimal doping concentration of  $\text{Er}^{3+}$  in the  $\alpha\text{-Na}_3\text{Y}(\text{VO}_4)_2$  is found to be 0.025 mol. The non-radiative interaction among  $\text{Er}^{3+}$  is attributed to the dipole–quadrupole interaction. The quantum yield is found to be 7.25%, and chromaticity coordinates for the optimal concentration are found to be (0.2571, 0.6707) which are close to National Television System Committee standards for green (0.21, 0.71). The lifetime of erbium emission is found to be in microsecond range. The photoluminescence studies reveal that the newly synthesized  $\text{Er}^{3+}$ -doped  $\alpha\text{-Na}_3\text{Y}(\text{VO}_4)_2$  nanocrystals would be a good choice as green emitter to be combined with previously investigated blue- and red-emitting  $\text{Tm}^{3+}$ - and  $\text{Sm}^{3+}$ -doped  $\alpha\text{-Na}_3\text{Y}(\text{VO}_4)_2$  nanocrystals for realizing RGB phosphor.

**Keywords** Vanadate · Erbium · Photoluminescence · Concentration quenching · Host sensitization

## 1 Introduction

Phosphor-converted (pc) WLED is rapidly replacing the conventional incandescent and fluorescence lamp in the field of general lighting and display backlight, owing to their surpassing benefits such as low energy consumption, low heat output, small footprints, spectral tunability, long lifetime as well as efficient conversion of electric power into optical power [1]. Coating of luminescent materials onto the surface of the UV/blue LED chip is the common method employed in improvising phosphor-converted WLED. This can be achieved by the combination of a blue LED with a yellow phosphor (YAG:Ce<sup>3+</sup>) or a combination of UV-LED with tricolor red, green and blue (RGB) phosphors or a combination of UV-LED with single-phased

white-emitting phosphors [2]. Among them, combination of UV-LED with single-phased tricolor-based white-emitting phosphors is significantly employed in WLED industry owing to their simplicity in operation, good luminous efficiency, low color correlated temperature (CCT), high color rendering index (CRI) and low manufacturing cost. A potential single-phased tricolor-based white phosphor with good absorption in the UV region, low correlated color temperature (CCT) and high color rendering index (CRI) is a matter of prime importance.

Among various rare earth-doped inorganic phosphors oxides, rare earth vanadates are an important class of luminescent materials. In addition to the good chemical stability, moisture resistance, inertness and eco-friendliness, rare earth-doped vanadates are attracting much attention due

✉ Cyriac Joseph, cyriacmgu@gmail.com | <sup>1</sup>School of Pure and Applied Physics, Mahatma Gandhi University, Kottayam 686560, India.

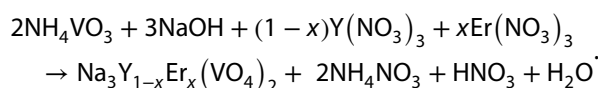


to their capacity to transfer energy from charge transfer band of vanadate to almost all luminescent rare earth ions efficiently ensuring intense characteristic emission in the entire visible range [3]. Rare earth ions are characterized by a partially filled 4f which is well screened by the 5s<sup>2</sup> and 5p<sup>6</sup> orbitals, yielding sharp emission lines especially in the visible region [4]. It is reported that yttrium vanadate single crystal can serve as laser host material [5] and Eu<sup>3+</sup>-doped yttrium vanadate has been used as commercial red phosphor in fluorescent lamp and cathode ray tube for last two decades [6, 7]. Rare earth-doped double vanadates of the form A<sub>3</sub>B(VO<sub>4</sub>)<sub>2</sub> (A denotes alkali metal like Na, K, Li and B represents La, Y, Gd) have attained significant attention in lighting applications [8, 9]. α-Na<sub>3</sub>Y(VO<sub>4</sub>)<sub>2</sub> has been selected as host lattice in this work, owing to their lower symmetry (C<sub>2v</sub>) occupied by Y<sup>3+</sup> ions in α-Na<sub>3</sub>Y(VO<sub>4</sub>)<sub>2</sub> compared to the D<sub>2d</sub> symmetry of Y<sup>3+</sup> ions in tetragonal YVO<sub>4</sub> [10]. We have already reported blue-emitting thulium-doped and reddish-orange-emitting samarium-doped α-Na<sub>3</sub>Y(VO<sub>4</sub>)<sub>2</sub> nanocrystals in which intense luminescence emission is achieved via host sensitization [11, 12]. The current work is a follow-up in search of a green-emitting rare earth-doped α-Na<sub>3</sub>Y(VO<sub>4</sub>)<sub>2</sub> in order to realize phosphors suitable for white light applications. Even though terbium is the commonly used green-emitting ion, terbium-doped α-Na<sub>3</sub>Y(VO<sub>4</sub>)<sub>2</sub> is not a proper choice to realize the green component in RGB phosphor since there is no significant energy transfer from vanadate band to terbium ion [13]. Therefore, the search for new green-emitting vanadate phosphor leads to the investigation on photoluminescence studies of Er<sup>3+</sup>-doped α-Na<sub>3</sub>Y(VO<sub>4</sub>)<sub>2</sub> nanocrystals. In this work, synthesis and photoluminescence characteristics of green-emitting erbium-doped α-Na<sub>3</sub>Y(VO<sub>4</sub>)<sub>2</sub> nanocrystalline phosphor are reported.

## 2 Experimental methods

### 2.1 Synthesis

Solution combustion method with citric acid as the fuel was employed for the synthesis of erbium-doped sodium yttrium vanadate [α-Na<sub>3</sub>Y<sub>1-x</sub>Er<sub>x</sub>(VO<sub>4</sub>)<sub>2</sub>] nanocrystals. A set of samples with varying erbium concentrations corresponding to x = 0, 0.01, 0.015, 0.02, 0.025, 0.03, 0.04, 0.05 were prepared. Sodium hydroxide (NaOH), ammonium vanadate (NH<sub>4</sub>VO<sub>3</sub>), ammonia solution, citric acid monohydrate (C<sub>6</sub>H<sub>8</sub>O<sub>7</sub>·H<sub>2</sub>O), high purity erbium (III) nitrate pentahydrate (Er(NO<sub>3</sub>)<sub>3</sub>·5H<sub>2</sub>O (99.99%)) and yttrium (III) nitrate hexahydrate (Y(NO<sub>3</sub>)<sub>3</sub>·6H<sub>2</sub>O (99.9%)) were used as the raw materials. All the chemicals used were of analytical grade. The chemical reaction leading to the formation of erbium-doped sodium yttrium vanadate is



Orthovanadate solution was prepared by mixing 10 ml aqueous solutions of 0.2 M NH<sub>4</sub>VO<sub>3</sub> and 0.3 M NaOH under stirring followed by heating at 70 °C for 1 h. 0.1 M aqueous solutions of Y(NO<sub>3</sub>)<sub>3</sub> and Er(NO<sub>3</sub>)<sub>3</sub> were mixed in the required stoichiometric ratio and added with citric acid keeping the ratio of total metal cations to citric acid as 1:4. This solution was then added drop wise into orthovanadate solution under stirring. The resulted yellowish orange solution was further heated at 80 °C for 1 h in a closed beaker and the color changed into blue. This solution was then allowed to evaporate by boiling at 120 °C for 1 h and was transferred into a muffle furnace and sintered at 500 °C for 2 h at the rate 300 °C/h and then allowed to cool. Fine powder of erbium-doped α-Na<sub>3</sub>Y(VO<sub>4</sub>)<sub>2</sub> nanocrystals thus formed were used for further analysis.

### 2.2 Characterization

X-ray powder diffraction patterns of the synthesized erbium-doped sodium yttrium vanadate samples were recorded in the 2θ range 10°–60° using Rigaku RU-200B X-ray diffractometer. Fourier transform infrared (FTIR) spectra of the samples were traced by a Shimadzu IR Prestige 20 spectrometer. Energy-dispersive X-ray spectrometry was employed to study the chemical composition of the sample using Carl Zeiss EVO 18 Secondary Electron Microscope with EDS. Transmission Electron Microscopic analysis was carried out using a JEOL JEM 2100 transmission electron microscope. The absorption spectra of the sample were recorded using Perkin Elmer Lambda 25 UV–Vis spectrometer in the wavelength range 200–800 nm. Photoluminescence excitation, emission and decay analysis were carried out on a Horiba Jobin–Yvon Fluoromax-4 spectrofluorometer.

## 3 Results and discussion

### 3.1 X-ray diffraction analysis

The X-ray diffraction patterns of erbium-doped sodium yttrium vanadate nanocrystals with varying erbium doping concentration are shown in Fig. 1. The well-defined diffraction peaks in the XRD profile ascertain the highly crystalline nature of prepared samples. The diffraction peaks of all the prepared samples match with that of pure α-Na<sub>3</sub>Y(VO<sub>4</sub>)<sub>2</sub> with monoclinic phase as per the standard data in ICDD file No. 55-0797. Table 1 represents the

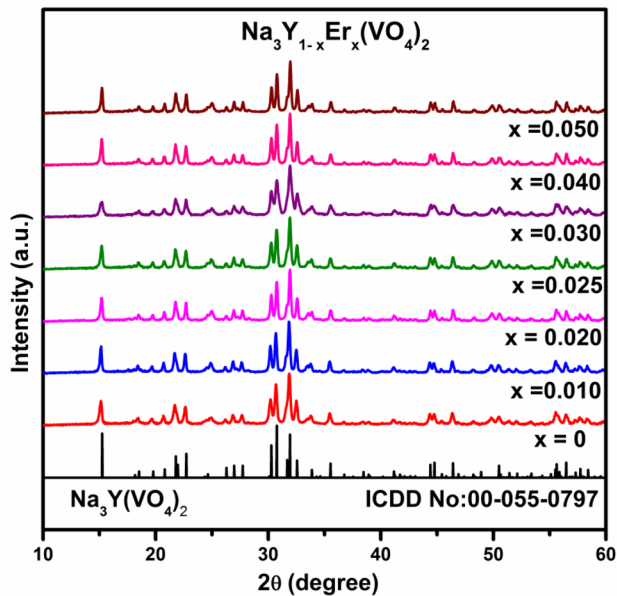


Fig. 1 XRD patterns of  $\alpha\text{-Na}_3\text{Y}_{1-x}\text{Er}_x(\text{VO}_4)_2$  nanocrystals

computed lattice parameters and the cell volume of the nanocrystals using the unit cell win software.

Close resemblance in the lattice parameters among various samples is ascribed due to the proximity in the ionic radii of yttrium (0.9 Å) and erbium (0.89 Å) with similar valences as well as due to the successful incorporation of erbium into the host lattice. Scherrer equation,  $D = \frac{0.9\lambda}{\beta \cos\theta}$ , has been employed to estimate average crystallite size of the sample, where  $D$  is the average crystallite size,  $\lambda$  is the X-ray wavelength (1.548 Å),  $\theta$  is the diffraction angle, and  $\beta$  is the full width half maximum (in radians) of the peak [14]. The estimated crystallite size of samples with various erbium concentrations is found to be in the range 22–33 nm and is also tabulated in Table 1.

$\alpha\text{-Na}_3\text{Y}(\text{VO}_4)_2$  is found to be iso-structural with monoclinic  $\alpha\text{-Na}_3\text{Er}(\text{VO}_4)_2$  with slightly distorted glasserite lattice with space group  $P2_1/n$ , No.14 and  $Z=2$ . Isolated  $\text{VO}_4^{3-}$  tetrahedra,  $\text{YO}_6$  and  $\text{NaO}_6$  octahedron constitute the crystal

structure of  $\alpha\text{-Na}_3\text{Y}(\text{VO}_4)_2$ . The site symmetry of  $\text{Y}^{3+}$  and  $\text{Er}^{3+}$  is  $C_{2v}$ , whereas  $\text{VO}_4^{3-}$  possesses the point symmetry of  $C_1$  [11]. The crystal structure has an effect on the luminescence properties of rare earth-doped  $\alpha\text{-Na}_3\text{Y}(\text{VO}_4)_2$ , and it is identified as an excellent phosphor for solid-state lighting applications.

### 3.2 Energy-dispersive X-ray analysis

The chemical purity of the sample is further verified by Energy-dispersive X-ray analysis, and the EDS spectrum of the sample  $\alpha\text{-Na}_3\text{Y}_{0.975}\text{Er}_{0.025}(\text{VO}_4)_2$  is shown in Fig. 2. The peaks present in the spectrum corresponding to sodium (Na), yttrium (Y), erbium (Er), vanadium (V), oxygen (O) validate the chemical composition and chemical purity of the samples.

### 3.3 Microstructural analysis

Figure 3 illustrates the microstructural features of  $\alpha\text{-Na}_3\text{Y}_{0.975}\text{Er}_{0.025}(\text{VO}_4)_2$  nanocrystals—a representative among the synthesized samples. TEM image shown in Fig. 3a indicates that the nanocrystals are of spherical shape and are well dispersed. The statistical particle distribution curve is plotted as shown in Fig. 3b, and the particle size is found to be in the range 10–50 nm. The formation of spherical

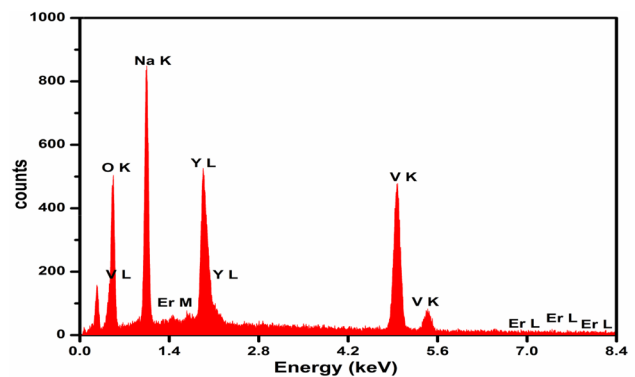
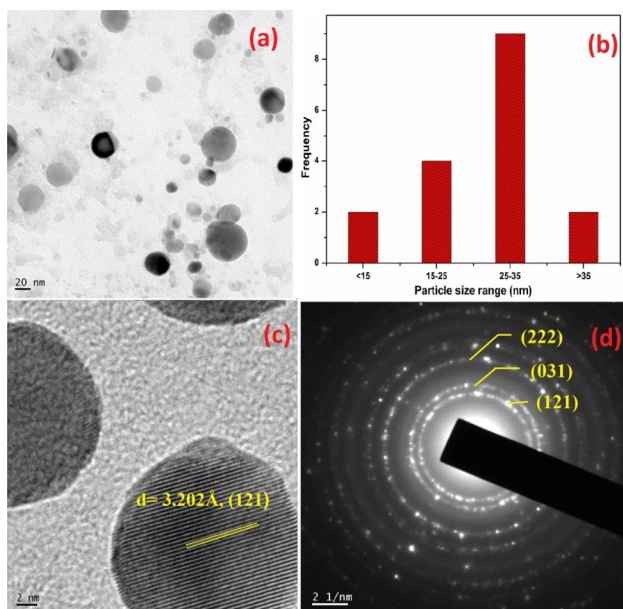


Fig. 2 EDS spectrum of  $\alpha\text{-Na}_3\text{Y}_{0.975}\text{Er}_{0.025}(\text{VO}_4)_2$  nanocrystals

Table 1 The lattice parameters of  $\alpha\text{-Na}_3\text{Y}_{1-x}\text{Er}_x(\text{VO}_4)_2$  nanocrystals

x	Lattice parameters				Cell volume (Å) <sup>3</sup>	Crystallite size (nm)
	a (Å)	b (Å)	c (Å)	β (°)		
0	7.2423	9.7785	5.5151	93.025	390.039	29.679
0.010	7.2423	9.7755	5.5153	92.988	389.934	25.664
0.020	7.2311	9.7725	5.4994	92.960	388.129	33.146
0.025	7.2331	9.7767	5.5004	93.001	388.089	23.897
0.030	7.2319	9.7662	5.5021	92.979	388.077	30.782
0.040	7.2293	9.7663	5.5023	92.987	387.960	32.221
0.050	7.2273	9.7671	5.4981	93.020	387.400	22.345



**Fig. 3** **a** TEM image, **b** particle distribution, **c** HRTEM image and **d** SAED pattern of  $\alpha\text{-Na}_3\text{Y}_{0.975}\text{Er}_{0.025}(\text{VO}_4)_2$  nanocrystals

nanocrystals is due to the presence of excess citric acid in confirmation with the previous reports [15].

Clear fringes in the HRTEM image corroborate the high crystalline nature of the  $\alpha\text{-Na}_3\text{Y}_{0.975}\text{Er}_{0.025}(\text{VO}_4)_2$  sample as shown in Fig. 3c. The presence of the (121) crystal planes corresponding to spacing  $d = 3.202 \text{ \AA}$  is recognized in the HRTEM image which is consistent with the XRD data. Selected area electron diffraction (SAED) image of  $\alpha\text{-Na}_3\text{Y}_{0.975}\text{Er}_{0.025}(\text{VO}_4)_2$  sample is displayed in Fig. 3d. Well-defined rings patterns are attributed to the polycrystalline nature of the sample. The planes (121), (031) and (222) which are associated with  $d = 3.19, 2.80$  and  $1.951 \text{ \AA}$ , respectively, are identified and are in close agreement with the standard ICDD of  $\alpha\text{-Na}_3\text{Y}(\text{VO}_4)_2$ .

### 3.4 Fourier transform infrared (FTIR) spectroscopy analysis

The vibrational modes in  $\alpha\text{-Na}_3\text{Y}_{1-x}\text{Er}_x(\text{VO}_4)_2$  where  $x = 0, 0.01, 0.02, 0.025, 0.030, 0.04, 0.05$  were identified from the FTIR spectrum displayed in Fig. 4. Tetrahedral  $\text{VO}_4^{3-}$  ion possesses  $T_d$  symmetry and has four normal modes of which only two are IR active. When the vanadate group becomes the part of monoclinic  $\alpha\text{-Na}_3\text{Y}(\text{VO}_4)_2$  lattice, the  $\text{VO}_4^{3-}$  group gets slightly distorted and the symmetry shifts to a lower one ( $C_1$ ) and all the fundamental modes become both IR and Raman active [16]. The bands below  $1000 \text{ cm}^{-1}$  are assigned due to internal vibration of the  $\text{VO}_4^{3-}$  ions. Strong bands observed at  $740 \text{ cm}^{-1}$  and  $960 \text{ cm}^{-1}$  are identified as  $\nu_3$  mode of

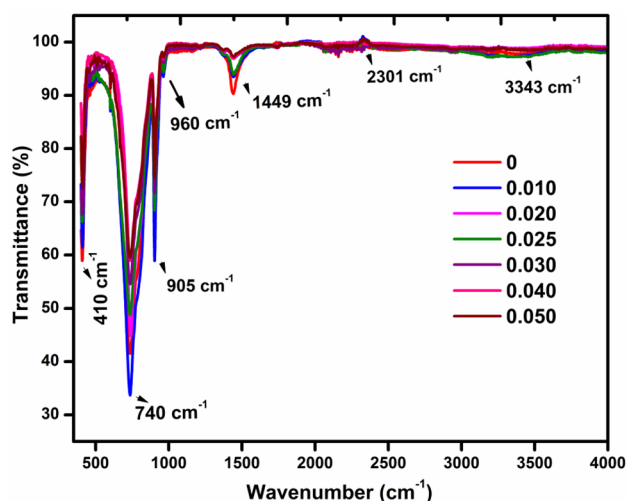


**Fig. 4** FTIR spectra of  $\alpha\text{-Na}_3\text{Y}_{1-x}\text{Er}_x(\text{VO}_4)_2$  nanocrystals

$\text{VO}_4^{3-}$ . The band at  $410 \text{ cm}^{-1}$  is attributed to  $\nu_2$  and  $\nu_4$  modes and that at  $905 \text{ cm}^{-1}$  as due to  $\nu_1$  mode of  $\text{VO}_4^{3-}$ . Feeble peaks at  $3343 \text{ cm}^{-1}$ ,  $2301 \text{ cm}^{-1}$  and  $1449 \text{ cm}^{-1}$  are due to the stretching and bending modes of OH vibrations and are less significant [17].

## 4 Optical characterization

### 4.1 UV–Vis absorption analysis

UV–Vis absorption spectra of erbium-doped  $\alpha\text{-Na}_3\text{Y}(\text{VO}_4)_2$  nanocrystals were recorded in order to have a better insight into the photoluminescence characteristics of the prepared phosphor. The absorption spectra in the range  $200\text{--}800 \text{ nm}$  for the samples with varying erbium concentration are depicted in Fig. 5. A strong and broad absorption band in the UV region is present in all the spectra attributing to the overlapped  $\text{O}^{2-}$  to  $\text{Er}^{3+}$  and  $\text{O}^{2-}$  to  $\text{V}^{5+}$  metal–ligand charge transfer transitions [18]. In the longer wavelength region (above  $350 \text{ nm}$ ), narrow absorption peaks due to f–f transitions of  $\text{Er}^{3+}$  are expected, but in the present case only a small peak is observed at  $522 \text{ nm}$  which is attributed to the transition from the ground state of erbium  $^4I_{15/2}$  to  $^2H_{11/2}$ . No other peaks are detected in the present case, may be due to the low doping content of  $\text{Er}^{3+}$  and pronounced intensity of host absorption band. The intense and broadband in the UV region is a promising pathway for energy transfer from vanadate host to erbium ions and offers flexibility in the choice of excitation wavelength in UV region.

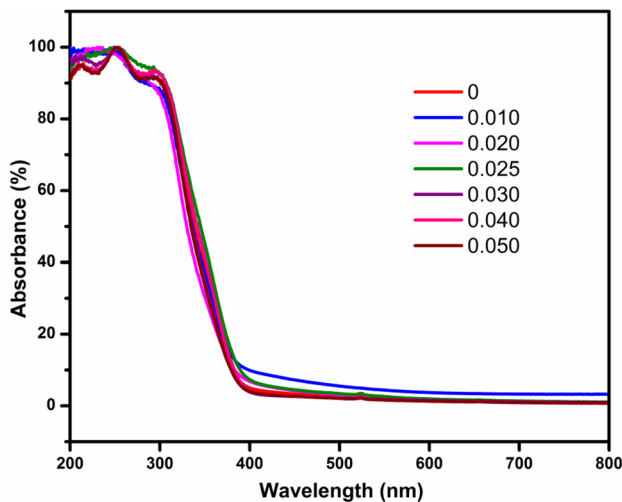


Fig. 5 UV-Vis absorption spectra of  $\alpha\text{-Na}_3\text{Y}_{1-x}\text{Er}_x(\text{VO}_4)_2$  nanocrystals

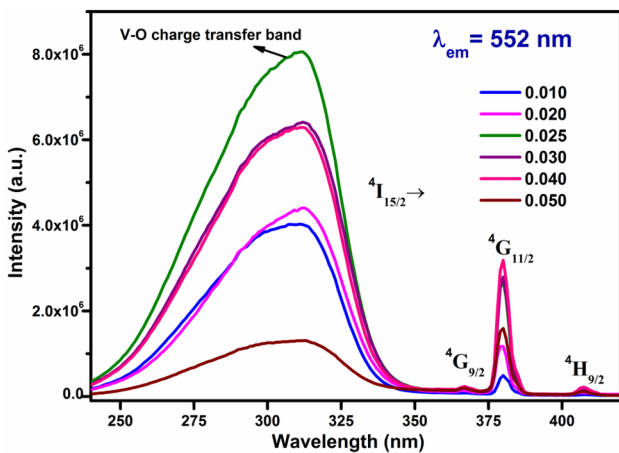


Fig. 6 Excitation spectra of  $\alpha\text{-Na}_3\text{Y}_{1-x}\text{Er}_x(\text{VO}_4)_2$  nanocrystals

## 4.2 Photoluminescence studies

The excitation spectra of  $\alpha\text{-Na}_3\text{Y}_{1-x}\text{Er}_x(\text{VO}_4)_2$  nanocrystals with a range of erbium concentrations corresponding to  $x=0.01, 0.02, 0.025, 0.030, 0.04, 0.05$  were recorded in the range 230–420 nm monitoring the 552 nm emission of  $\text{Er}^{3+}$  and are displayed in Fig. 6. The broadband peaked around 310 nm arises due to the charge transfer transitions [19]. The sharp peaks at 366 nm, 380 nm and 407 nm are assigned, respectively, due to  ${}^4\text{I}_{15/2} \rightarrow {}^4\text{G}_{9/2}$ ,  ${}^4\text{I}_{15/2} \rightarrow {}^4\text{G}_{11/2}$  and  ${}^4\text{I}_{15/2} \rightarrow {}^4\text{H}_{9/2}$  transitions of  $\text{Er}^{3+}$  ion [20]. The appearance of strong and extended excitation peak in the UV range on monitoring the emission of  $\text{Er}^{3+}$  ascertains the sensitization of erbium via host.

Figure 7 illustrates the photoluminescence emission spectra of  $\alpha\text{-Na}_3\text{Y}_{1-x}\text{Er}_x(\text{VO}_4)_2$  where  $x=0.01, 0.02, 0.025,$

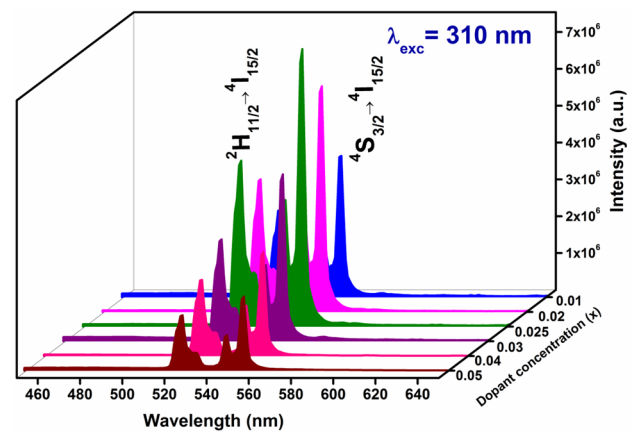


Fig. 7 Emission spectra of  $\alpha\text{-Na}_3\text{Y}_{1-x}\text{Er}_x(\text{VO}_4)_2$  nanocrystals

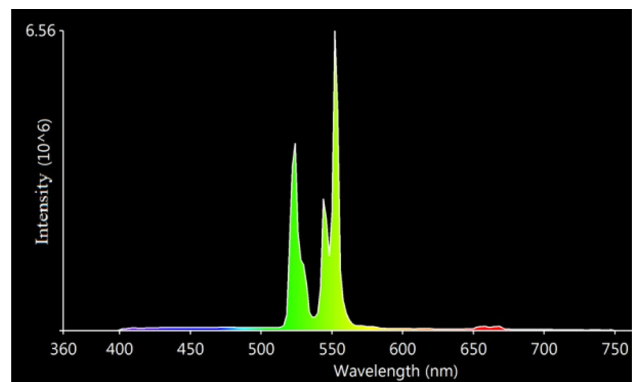
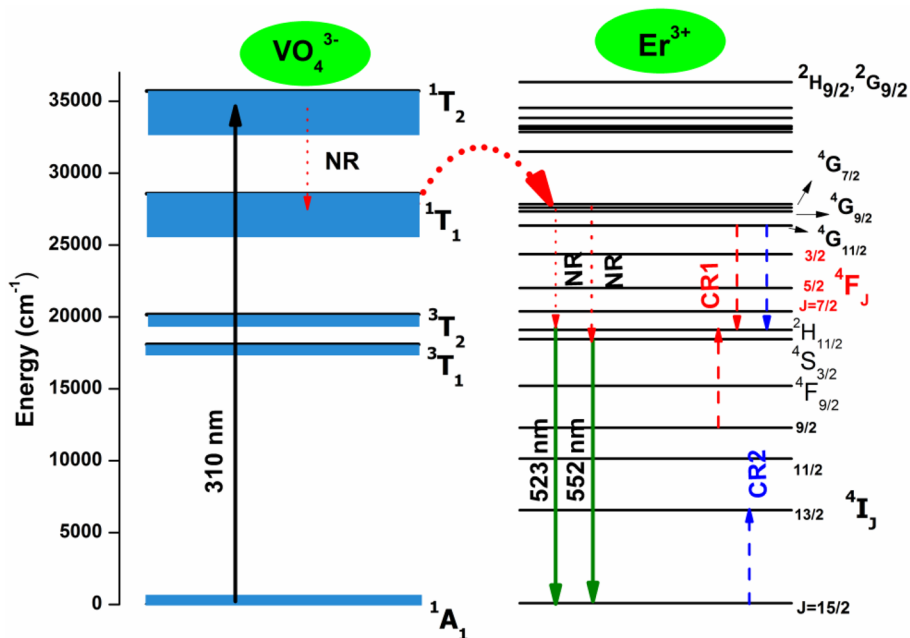


Fig. 8 Emission spectrum of  $\alpha\text{-Na}_3\text{Y}_{0.975}\text{Er}_{0.025}(\text{VO}_4)_2$  nanocrystals

0.030, 0.04, 0.05 under 310 nm host excitation. Green emission centered at 523 nm and 552 nm was detected and attributed to the transitions from  ${}^2\text{H}_{11/2}$  and  ${}^4\text{S}_{3/2}$  levels to the  ${}^4\text{I}_{15/2}$  ground state, respectively. Violet emission around 408 nm ( ${}^2\text{H}_{9/2} \rightarrow {}^4\text{I}_{15/2}$ ) and red emission around 660 nm ( ${}^4\text{F}_{9/2} \rightarrow {}^4\text{I}_{15/2}$ ) were hardly visible revealing the efficient non-radiative relaxation from  ${}^2\text{H}_{9/2}$  and  ${}^4\text{F}_{9/2}$  [20]. The prevalent green emission in the emission spectra as depicted in Fig. 8 brings out  $\alpha\text{-Na}_3\text{Y}_{1-x}\text{Er}_x(\text{VO}_4)_2$  nanocrystal as an excellent green phosphor with better chromaticity for white light generation.

Various radiative and non-radiative pathways involved in the photoluminescence mechanism of  $\text{Er}^{3+}$  in  $\alpha\text{-Na}_3\text{Y}(\text{VO}_4)_2$  is picturized in the schematic energy level diagram as shown in Fig. 9. Vanadate ion in  ${}^1\text{A}_1$  ground state could be excited to  ${}^1\text{T}_2$  state upon excitation at 310 nm and then non-radiatively relaxed to  ${}^1\text{T}_1$  state. The  ${}^1\text{T}_1$  excited state energy of vanadate is almost the same as that of  ${}^4\text{G}_{7/2}$  excited state of  $\text{Er}^{3+}$  resulting in non-radiative resonant energy transfer from vanadate to  $\text{Er}^{3+}$  ions. The  ${}^4\text{G}_{7/2}$  excited state of  $\text{Er}^{3+}$  gets depopulated non-radiatively

**Fig. 9** Energy level diagram representing photoluminescence mechanism in  $\alpha\text{-Na}_3\text{Y}_{1-x}\text{Er}_x(\text{VO}_4)_2$



into  $^2\text{H}_{11/2}$  and  $^4\text{S}_{3/2}$  emitting state of  $\text{Er}^{3+}$  ions which trigger the green emission around 523 nm and 552 nm, respectively. The possible non-radiative cross-relaxation channels responsible for concentration quenching are  $^4\text{I}_{9/2} + ^4\text{G}_{11/2} \rightarrow ^2\text{H}_{11/2} + ^2\text{H}_{11/2}$  or  $^4\text{S}_{3/2}$  and  $^4\text{I}_{15/2} + ^4\text{G}_{11/2} \rightarrow ^4\text{I}_{13/2} + ^2\text{H}_{11/2}$  or  $^4\text{S}_{3/2}$  and are represented as CR1 and CR2, respectively, in Fig. 9 [21].

Photoluminescence emission spectra of the samples (Fig. 7) also show that the intensity of green emission goes on increasing with the increase in doping concentration  $\text{Er}^{3+}$  up to the optimal concentration  $x=0.025$  mol and then decreases in tune with the trend observed in the excitation spectra. The plot of intensity of 552 nm emission versus  $\text{Er}^{3+}$  concentration when excited at 310 nm is displayed in Fig. 10. A sudden fall in luminescence intensity on increasing  $\text{Er}^{3+}$  content beyond  $x=0.025$  mol arises from the concentration quenching effects due to non-radiative cross-relaxation path and the energy transfer among  $\text{Er}^{3+}$  ions until energy sink in the lattice is reached.

The type of non-radiative energy transfer among  $\text{Er}^{3+}$  ions that leads to concentration quenching strongly depends on the critical distance ( $R_c$ ) between adjacent  $\text{Er}^{3+}$  ions. The critical distance ( $R_c$ ) between adjacent  $\text{Er}^{3+}$  ions as provided by the following Blasse equation is

$$R_c = 2 \left( \frac{3V}{4\pi x_c N} \right)^{\frac{1}{3}}$$

where  $V$  is the unit cell volume,  $N$  is the number of  $\text{Er}^{3+}$  ions in a unit cell,  $x_c$  is the optimal concentration, and the critical distance is calculated to be about 24.55 Å [22]. If the critical distance ( $R_c$ ) between adjacent  $\text{Er}^{3+}$  ions is

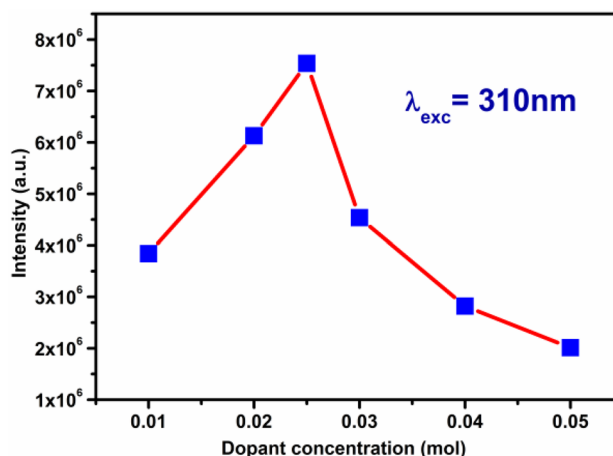


**Fig. 10** Intensity of green emission at 552 nm versus  $\text{Er}^{3+}$  concentration

less than 5 Å, the interaction is mainly exchange interaction whereas the critical distance ( $R_c$ ) is greater than 5 Å, multipolar interaction is responsible for concentration quenching. The type of multipolar interaction can be identified using Dexter’s formula [23].

$$\log(I/C) = K - (Q/3) \log(C)$$

where  $I$  is the intensity corresponding to the doping concentration ( $C$ ).  $Q$  represents the type of multipolar interaction and  $Q=6, 8, 10$  correspond to the dipole–dipole, dipole–quadrupole and quadrupole–quadrupole interactions, respectively.  $\log(I/C) - \log(C)$  curve is plotted for different  $\alpha\text{-Na}_3\text{Y}_{1-x}\text{Er}_x(\text{VO}_4)_2$  nanocrystals ( $x=0.01$ ,

0.02, 0.025, 0.030, 0.04, 0.05) for green emission (552 nm) excited at 310 nm and is found to be linear as depicted in Fig. 11. The value of  $Q$  is calculated as 8.57 which indicates that the non-radiative energy transfer among  $\text{Er}^{3+}$  ions is caused by dipole–quadrupole interaction. The quantum yield of the  $\alpha\text{-Na}_3\text{Y}_{1-x}\text{Er}_x(\text{VO}_4)_2$  nanocrystals with  $x=0.025$  is found to be 7.25% and comparable with earlier reported cases [24].

### 4.3 Luminescence decay analysis

Figure 12a displays the decay curves of  $\alpha\text{-Na}_3\text{Y}_{1-x}\text{Er}_x(\text{VO}_4)_2$  nanocrystals ( $x=0, 0.01, 0.025$  and  $0.05$ ) monitoring the host emission at 438 nm on exciting at 310 nm. All the decay curves of host emission are found to be double exponential, and the luminescence emission

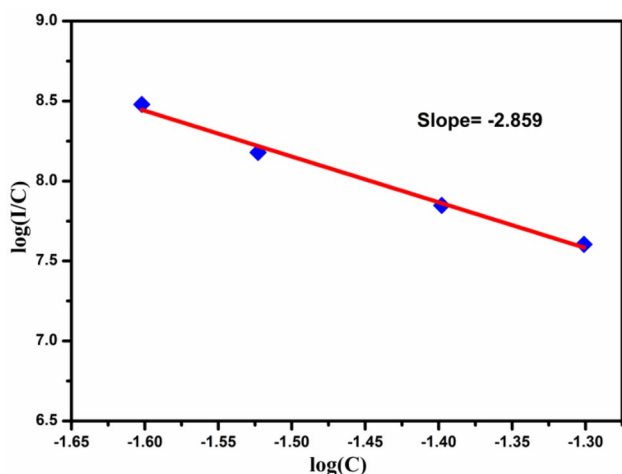


Fig. 11  $\log(I/C)$  versus  $\log(C)$  curve

persists up to 80  $\mu\text{s}$ . The short lifetimes are found to be 0.616, 0.554 and 0.553  $\mu\text{s}$ , and the long lifetimes are 12.393, 11.571, 10.99  $\mu\text{s}$  for erbium concentrations  $x=0.01, 0.025$  and  $0.05$ , respectively. This double exponential decay nature indicates energy transfer from vanadate to erbium. The average lifetime of the host emission is calculated using the formula  $t_{\text{avg}} = \frac{A_1 t_1^2 + A_2 t_2^2}{A_1 t_1 + A_2 t_2}$ , where  $t_1$  and  $t_2$  are the lifetime values and  $A_1$  and  $A_2$  are the corresponding weight factors. The calculated average lifetime values are 10.128, 9.067 and 8.663  $\mu\text{s}$  corresponding to erbium concentrations  $x=0.01, 0.025$  and  $0.05$ , respectively.

The decay curves of 552 nm erbium emission monitored upon 310 nm excitation are shown in Fig. 12b. The nature of the decay curves seems to be multi-exponential by appearance on account of the very slow decay in the beginning of the curve. But the decay curves are best fitted to single exponential in nature, since the slow decay in the beginning of the curve is less significant considering the general nature of the decay process. The lifetime values obtained by the single exponential fitting are 11.045, 10.519 and 10.466  $\mu\text{s}$  corresponding to erbium concentrations  $x=0.01, 0.025$  and  $0.05$ , respectively, matching with similar reports [25]. The slight decrease in the lifetime values is due to the luminescence quenching due to the interaction among the  $\text{Er}^{3+}$  ions. The energy transfer efficiency from vanadate to erbium in  $\alpha\text{-Na}_3\text{Y}_{1-x}\text{Er}_x(\text{VO}_4)_2$  nanocrystals ( $x=0.01, 0.025$  and  $0.05$ ) was calculated as 40.725, 53.285 and 56.385% using the equation  $\eta_{\text{ET}} = 1 - \frac{\tau_s}{\tau_0}$ , where  $\tau_0$  and  $\tau_s$  refer to the lifetime of vanadate emission without the activator  $\text{Er}^{3+}$  and with  $\text{Er}^{3+}$  ions, respectively, on host excitation 310 nm.

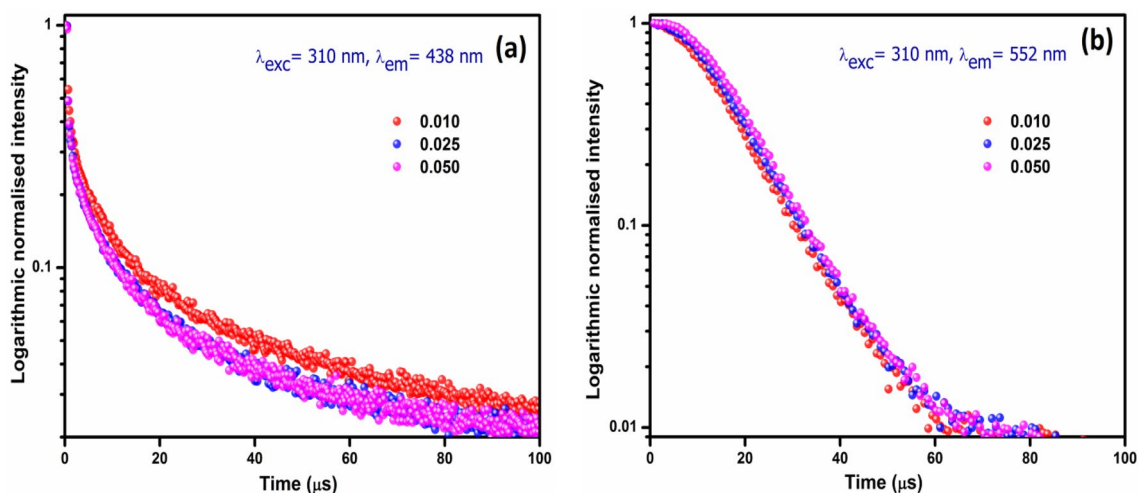
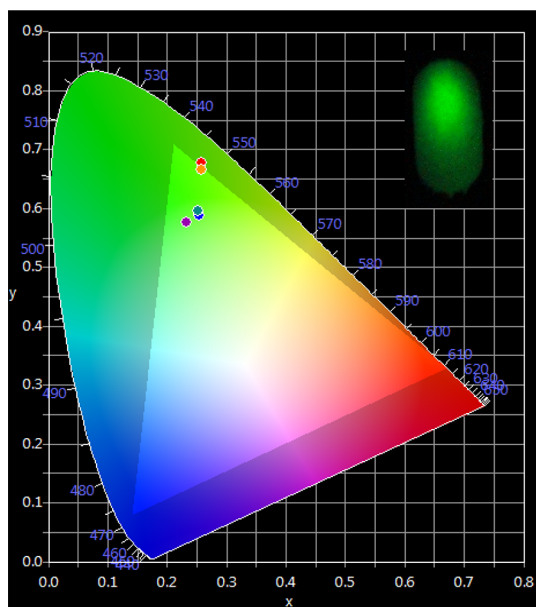


Fig. 12 Decay curves of **a** host emission at 438 nm, **b**  $\text{Er}^{3+}$  emission at 552 nm of  $\alpha\text{-Na}_3\text{Y}_{1-x}\text{Er}_x(\text{VO}_4)_2$  nanocrystals



**Fig. 13** CIE chromaticity diagram of  $\alpha\text{-Na}_3\text{Y}_{1-x}\text{Er}_x(\text{VO}_4)_2$  nanocrystals ( $x=0.01, 0.02, 0.025, 0.030, 0.04, 0.05$ ). The inset shows digital photograph of the sample under 310 nm excitation

**Table 2** The CIE chromaticity coordinates of  $\alpha\text{-Na}_3\text{Y}_{1-x}\text{Er}_x(\text{VO}_4)_2$  nanocrystals

Doping concentration ( $x$ )	CIE chromaticity coordinates	
	$x$	$y$
0.010	0.2540	0.5877
0.020	0.2571	0.6767
0.025	0.2574	0.6662
0.030	0.2517	0.5949
0.040	0.2407	0.6560
0.050	0.2322	0.5771

#### 4.4 Colorimetric analysis

In order to have a better understanding on the quality of emitting color of the phosphor which is very significant in various lighting applications, CIE colorimetric studies can be employed. The Commission Internationale de l'Éclairage chromaticity diagram of  $\alpha\text{-Na}_3\text{Y}_{1-x}\text{Er}_x(\text{VO}_4)_2$  (where  $x=0.01, 0.02, 0.025, 0.030, 0.04, 0.05$ ) nanocrystalline phosphors under 310 nm excitation was plotted using the color calculator software and is exhibited in Fig. 13. The corresponding digital photograph of  $\alpha\text{-Na}_3\text{Y}_{1-x}\text{Er}_x(\text{VO}_4)_2$  ( $x=0.025$ ) is shown in the inset of Fig. 13. The chromaticity coordinates of the samples were evaluated and are tabulated in Table 2 [26]. The CIE chromaticity coordinates of  $\alpha\text{-Na}_3\text{Y}_{0.975}\text{Er}_{0.025}(\text{VO}_4)_2$  (0.25, 0.67) are found to be very close to National Television System Committee (NTSC) standard green (0.21, 0.71) as well as European

broadcasting union (EBU) standard green (0.29, 0.60) with high color purity (84%).

#### 4.5 Conclusion

Erbium-activated  $\alpha\text{-Na}_3\text{Y}(\text{VO}_4)_2$  was synthesized via fast and facile low temperature citrate-based solution combustion method. X-ray diffraction studies confirmed the monoclinic phase of the sample and the chemical composition is validated by EDS analysis. FTIR studies also confirmed the formation of  $\alpha\text{-Na}_3\text{Y}(\text{VO}_4)_2$  phase by observing the characteristic peaks. The highly crystalline nature and uniform spherical morphology of the sample were revealed by TEM analysis. Efficient energy transfer from host to  $\text{Er}^{3+}$  is proposed on the basis of UV–Vis absorption and photoluminescence excitation studies. Under 310 nm host excitation,  $\alpha\text{-Na}_3\text{Y}_{1-x}\text{Er}_x(\text{VO}_4)_2$  nanocrystals exhibit intense green emission around 523 nm and 552 nm corresponding to the transitions  ${}^2\text{H}_{11/2} \rightarrow {}^4\text{I}_{15/2}$  and  ${}^4\text{S}_{3/2} \rightarrow {}^4\text{I}_{15/2}$  of  $\text{Er}^{3+}$ , respectively. The quantum yield of the sample is found to be 7.25%, and energy transfer efficiency is calculated as 56% for optimum concentration of erbium. The lifetime of erbium emission in  $\alpha\text{-Na}_3\text{Y}_{1-x}\text{Er}_x(\text{VO}_4)_2$  is found to be in the microsecond range. From the CIE chromaticity diagram, the potential of  $\alpha\text{-Na}_3\text{Y}_{1-x}\text{Er}_x(\text{VO}_4)_2$  nanocrystals as a green phosphor with high color purity (84%) is ensured. The proximity of the chromaticity coordinate values of the above sample with the NTSC and EBU standards makes it suitable for developing single wavelength excitable phosphor-converted white LED applications.

**Acknowledgements** Linju Ann Jacob, first author of this research paper, is extremely grateful to UGC, Govt. of India for providing financial support through faculty development program). Mrs. Sisira S, Mrs. Kukku Thomas and Mrs. Dinu Alexander are thankful for the award of research fellowships to CSIR, Govt. of India (JRF fellowship), UGC, Govt. of India (MANF fellowship) and UGC, Govt. of India (RFSMS fellowship), respectively. The authors are thankful to Department of Science and Technology, Govt. of India and for the support through the programs of SAP-DRS (No. F.530/12/DRS/2009 (SAP-1)) and DST-PURSE (SR/417&418/2017)), respectively. A special thanks to MoU-DAE-BRNS Project (No. 2009/34/36/BRNS/3174) and to department of Physics, St. Thomas College, Palai, India, for extending their experimental facility.

#### Compliance with ethical standards

**Conflict of interest** The authors declare that they have no conflict of interest.

#### References

1. Smet PF, Joos JJ (2017) White light-emitting diodes: stabilizing colour and intensity. *Nat Mater* 16:500–501. <https://doi.org/10.1038/nmat4901>



- Vishwakarma AK, Jha K, Jayasimhadri M, Sivaiah B, Gahtori B, Haranath D (2015) Emerging cool white light emission from Dy<sup>3+</sup> doped single phase alkaline earth niobate phosphors for indoor lighting applications. *Dalt Trans* 44:17166–17174. <https://doi.org/10.1039/c5dt02436f>
- Huang X, Guo H (2018) Synthesis and photoluminescence properties of Eu<sup>3+</sup>-activated LiCa<sub>3</sub>ZnV<sub>3</sub>O<sub>12</sub> white-emitting phosphors. *RSC Adv* 8:17132–17138. <https://doi.org/10.1039/c8ra03075h>
- Blasse G, Grabmaier BC, Blasse G, Grabmaier BC (2011) A general introduction to luminescent materials. *Lumin Mater*. [https://doi.org/10.1007/978-3-642-79017-1\\_1](https://doi.org/10.1007/978-3-642-79017-1_1)
- Morrison AD (1973) Note on inclusions in yttrium vanadate crystals. *J Mater Sci* 8:1666–1669. <https://doi.org/10.1007/BF00754903>
- Palilla FC (1964) A new, highly efficient red-emitting cathodoluminescent phosphor (YVO<sub>4</sub>:Eu) for color television. *Appl Phys Lett* 5:118–120. <https://doi.org/10.1063/1.1723611>
- Levine AK, Palilla FC (1965) YVO<sub>4</sub>:Eu-A 10 New red-emitting phosphor for color television. *Trans N Y Acad Sci* 27:517–529. <https://doi.org/10.1111/j.2164-0947.1965.tb02210.x>
- David ADJ, Muhammad GS, Sivakumar V (2016) Synthesis and photoluminescence properties of Sm<sup>3+</sup>-substituted glaserite-type orthovanadates K<sub>3</sub>[VO<sub>4</sub>]<sub>2</sub> with monoclinic structure. *J Lumin* 177:104–110. <https://doi.org/10.1016/j.jlumin.2016.04.025>
- Hussain SK, Giang TTH, Yu JS (2018) UV excitation band induced novel Na<sub>3</sub>Gd(VO<sub>4</sub>)<sub>2</sub>:RE<sup>3+</sup> (RE<sup>3+</sup> = Eu<sup>3+</sup> or Dy<sup>3+</sup> or Sm<sup>3+</sup>) double vanadate phosphors for solid-state lightning applications. *J Alloys Compd* 739:218–226. <https://doi.org/10.1016/j.jallcom.2017.12.200>
- Miller SA, Caspers HH, Rast HE (1968) Lattice vibrations of Yttrium Vanadate. *Phys Rev* 168:964–969. <https://doi.org/10.1103/PhysRev.168.964>
- Jacob LA, Sisira S, Mani KP, Thomas K, Alexander D, Biju PR, Unnikrishnan NV, Joseph C (2020) High purity blue photoluminescence in thulium activated α-Na<sub>3</sub>Y(VO<sub>4</sub>)<sub>2</sub> nanocrystals via host sensitization. *J Lumin* 223:117169. <https://doi.org/10.1016/j.jlumin.2020.117169>
- Jacob LA, Sisira S, Thomas K, Alexander D, Biju PR, Unnikrishnan NV, Joseph C (2019) A reddish-orange emitting samarium doped α-Na<sub>3</sub>Y(VO<sub>4</sub>)<sub>2</sub> nanocrystals for single phased UV excitable white light applications. *J Solid State Chem* 280:120998. <https://doi.org/10.1016/j.jssc.2019.120998>
- Huang P, Chen D, Wang Y (2011) Host-sensitized multicolor tunable luminescence of lanthanide ion doped one-dimensional YVO<sub>4</sub> nano-crystals. *J Alloys Compd* 509:3375–3381. <https://doi.org/10.1016/j.jallcom.2010.12.069>
- Patterson AL (1939) The scherrer formula for X-ray particle size determination. *Phys Rev* 56:978–982. <https://doi.org/10.1103/PhysRev.56.978>
- Du G, Kan X, Han Y, Sun Z, Guo W (2012) Citric acid assisted hydrothermal synthesis of microparticles of ErPO<sub>4</sub>:Dy<sup>3+</sup>. *Mater Lett* 79:55–57. <https://doi.org/10.1016/j.matlet.2012.03.086>
- Sobczyk M (2013) Optical properties of α-Nd<sup>3+</sup>: Na<sub>3</sub>Y(VO<sub>4</sub>)<sub>2</sub> single crystals-Potential laser materials. *Opt Mater (Amst)* 35:852–859. <https://doi.org/10.1016/j.optmat.2012.10.043>
- Rao BV, Jang K, Sueb H, Yi S, Jeong J (2010) Synthesis and photoluminescence characterization of RE<sup>3+</sup> (= Eu<sup>3+</sup>, Dy<sup>3+</sup>) -activated Ca<sub>3</sub>La(VO<sub>4</sub>)<sub>3</sub> phosphors for white light-emitting diodes. *J Alloys Compd* 496:251–255. <https://doi.org/10.1016/j.jallcom.2009.12.175>
- Zhang Q, Hu Y, Ju G, Zhang S, Xue F (2017) Photoluminescence of a novel Na<sub>3</sub>Y(VO<sub>4</sub>)<sub>2</sub>:Eu<sup>3+</sup> red phosphor for near ultraviolet light emitting diodes application. *J Mater Sci: Mater Electron* 28:2529–2537. <https://doi.org/10.1007/s10854-016-5827-0>
- Kimani MM, Kolis JW (2014) Synthesis and luminescence studies of a novel white Dy:K<sub>3</sub>Y(VO<sub>4</sub>)<sub>2</sub> and yellow emitting phosphor Dy,Bi:K<sub>3</sub>Y(VO<sub>4</sub>)<sub>2</sub> with potential application in white light emitting diodes. *J Lumin* 145:492–497. <https://doi.org/10.1016/j.jlumin.2013.07.054>
- Yan SA, Wang JW, Chang YS, Hwang WS, Chang YH (2011) Synthesis and luminescence properties of Ln<sup>3+</sup> (Ln<sup>3+</sup> = Er<sup>3+</sup>, Sm<sup>3+</sup>)-doped barium lanthanum tungstate BaLa<sub>2</sub>WO<sub>7</sub> phosphors. *Opt Mater (Amst)* 34:147–151. <https://doi.org/10.1016/j.optmat.2011.07.028>
- Song F, Zhang G, Shang M, Tan H, Yang J, Meng F (2001) Three-photon phenomena in the upconversion luminescence of erbium–ytterbium codoped phosphate glass. *Appl Phys Lett* 79:1748. <https://doi.org/10.1063/1.1404996>
- Blasse G (1968) Energy transfer in oxidic phosphors. *Phys Lett A* 28:444–445. [https://doi.org/10.1016/0375-9601\(68\)90486-6](https://doi.org/10.1016/0375-9601(68)90486-6)
- Dexter DL (1953) A theory of sensitized luminescence in solids. *J Chem Phys* 21:836–850. <https://doi.org/10.1063/1.1699044>
- Pokhrel M, Kumar GA, Ma C, Brik M, Langloss B, Shanton I, Therien MJ, Sardar D, Mao Y (2015) Electronic and optical properties of Er: doped Y<sub>2</sub>O<sub>3</sub>S phosphors. *J Mater Chem C* 3(43):11486–11496. <https://doi.org/10.1039/C5TC02665B>
- Sreeja E, Mohan RP, Gopi S, Joseph C, Unnikrishnan NV, Biju PR (2019) Structural and photoluminescence properties of UV-excited Er<sup>3+</sup> doped Ba<sub>2</sub>CaWO<sub>6</sub> yellowish-green phosphors. *Phys B Condens Matter* 555:284–291. <https://doi.org/10.1016/j.physb.2018.11.020>
- Smith T, Guild J (1931) The C.I.E. colorimetric standards and their use. *Trans Opt Soc* 33:73–134

**Publisher's Note** Springer Nature remains neutral with regard to jurisdictional claims in published maps and institutional affiliations.